Article

Natural Organic Matter Concentration Impacts the Interaction of Functionalized Diamond Nanoparticles with Model and Actual Bacterial Membranes

Arielle C. Mensch, Rodrigo Tapia Hernandez, Joshua E. Kuether, Marco D. Torelli, Z. Vivian Feng, Robert J Hamers, and Joel A. Pedersen

Environ. Sci. Technol., **Just Accepted Manuscript** • DOI: 10.1021/acs.est.7b02823 • Publication Date (Web): 17 Aug 2017

Natural Organic Matter Concentration Impacts the Interaction of Functionalized Diamond Nanoparticles with Model and Actual Bacterial Membranes

Arielle C. Mensch[1], Rodrigo Tapia Hernandez[2], Joshua E. Kuether[2], Marco D. Torelli[1,a], Z. Vivian Feng[2], Robert J. Hamers[1], and Joel A. Pedersen[*,1,3,4]

[1] Department of Chemistry, University of Wisconsin, Madison, WI 53706, United States

[2] Chemistry Department, Augsburg College, Minneapolis, MN 55454, United States

[3] Department of Soil Science, University of Wisconsin, Madison, WI 53706, United States

[4] Department of Civil and Environmental Engineering, University of Wisconsin, Madison, WI 53706, United States

ABSTRACT: Changes to nanoparticle surface charge, colloidal stability, and hydrodynamic properties induced by interaction with natural organic matter (NOM) warrant consideration in assessing the potential for these materials to adversely impact organisms in the environment. Here we show that acquisition of a coating, or "corona", of NOM alters the hydrodynamic and electrokinetic properties of diamond nanoparticles (DNPs) functionalized with the polycation poly(allylamine HCl) in a manner that depends on the NOM-to-DNP concentration ratio. The NOM-induced changes to DNP properties alter subsequent interactions with model biological membranes and the Gram-negative bacterium *Shewanella oneidensis* MR-1. Suwannee River NOM induces changes to DNP hydrodynamic diameter and apparent ζ-potential in a concentration-dependent manner. At low NOM-to-DNP ratios, DNPs aggregate to a limited extent but retain a positive ζ-potential apparently due to non-uniform adsorption of NOM molecules leading to attractive electrostatic interactions between oppositely charged regions on adjacent DNP surfaces. Diamond nanoparticles at low NOM-to-DNP ratios attach to model membranes to a larger extent than in the absence of NOM (including those incorporating

lipopolysaccharide, a major bacterial outer membrane component) and induce a comparable degree of membrane damage and toxicity to *S. oneidensis*. At higher NOM-to-DNP ratios, DNP charge is reversed, and DNP aggregates remain stable in suspension. This charge reversal eliminates DNP attachment to model membranes containing the highest LPS contents studied due to electrostatic repulsion and abolishes membrane damage to *S. oneidensis*. Our results demonstrate that the effects of NOM coronas on nanoparticle properties and interactions with biological surfaces can depend on the relative amounts of NOM and nanoparticles.

INTRODUCTION

Rapid growth in the production and use of engineered nanomaterials has been accompanied by an increase in the potential for these materials to be released into the environment and for organisms to be exposed to them.[1-2] The large surface-to-volume ratio of nanomaterials as well as their high surface energy promotes the acquisition of a coating or "corona" of natural organic matter (NOM)[3-5] upon entry into wastewater treatment plants, natural waters, aquatic sediments, and soils. Natural organic matter is comprised of a complex mixture of relatively low molecular mass organic compounds resulting primarily from microbial degradation of vegetation, algae, and bacterial biomass.[6] Natural organic matter is found in natural waters at organic carbon (oc) concentrations ranging from ~0.5 $mg_{oc} \cdot L^{-1}$ in seawater and groundwater to over 30 $mg_{oc} \cdot L^{-1}$ in wetlands.[7] Over the pH range typical for environmental systems (4 to 9), NOM bears a net negative charge due to the deprotonation of carboxyl and phenolic groups.[8-9] Acquisition of a NOM "corona" alters the physical and chemical properties of nanomaterials and impacts their transport and fate in the environment.[10-13] Interaction with NOM can stabilize nanoparticle suspensions electrostatically or through a combination of electrostatic and steric interactions.[13] Natural organic matter can induce aggregation of

nanoparticles in the presence of elevated concentrations of divalent metal cations and when neutralizing nanoparticle charge.[14-16] Such nanoparticle aggregation in the presence of NOM depends on the nanoparticle coating,[14,17] NOM properties (e.g., polarity fraction,[18-21] molecular mass[22-25]), and NOM concentration.[16,26-27] Natural organic matter-induced changes to nanoparticle surface charge, colloidal stability, and hydrodynamic properties warrant consideration in assessing the potential for these materials to adversely impact organisms in the environment.

The initial point of contact between nanoparticles and cells is often a lipid membrane, yet the impact of NOM on nanoparticle interactions with cell membranes has received little study. One previous study showed that humic acid decreased fullerene accumulation in zwitterionic and negatively charged solid-supported lipid membranes and reduced uptake by Caco-2 cells.[28] The reduction in cellular uptake was attributed to electrostatic repulsion between the negatively charged humic acid-coated fullerene surface and the negatively charged Caco-2 cytoplasmic membrane.[28] Similarly, NOM prevented adhesion of nanoscale zero-valent iron to the outer membrane of *Escherichia coli* through electrostatic and steric repulsion, decreasing toxicity.[29] These studies demonstrate that NOM coatings can modulate the interaction of nanoparticles with cellular membranes.

Solid-supported lipid bilayers are often used as model systems to understand the complex interactions that occur between nanomaterials and cellular membranes.[30-36] The majority of these studies have employed bilayers composed of a single phospholipid or binary mixtures of phospholipids. Such bilayers do not include cell surface components expected to be important for the interaction of nanoparticles with bacteria. For example, the outer membrane of Gram-negative bacteria is complex and its outer leaflet contains up to 75% lipopolysaccharides

(LPS), a class of glycolipids.[37] The construction of model membranes incorporating LPS has been recently reported.[33,38] Nanoparticle interactions with model membranes incorporating LPS are expected to correspond more closely to results obtained using bacteria than are those with bilayers lacking these important cell-surface molecules.[33] Identification of the impacts of NOM on nanoparticle hydrodynamic and electrokinetic properties as well as on their interactions with model and actual bacterial membranes is needed to better elucidate the role NOM plays in interactions between nanomaterials and bacteria.

The objectives of this study were to investigate the impact of NOM-to-nanoparticle concentration ratio on the interaction of cationic nanoparticles with model cell membranes, including those incorporating LPS, and with the Gram-negative bacterium *Shewanella oneidensis* MR-1. To achieve these objectives, we used diamond nanoparticles (DNPs) functionalized with the polycation poly(allylamine HCl) (PAH) and Suwannee River NOM as model systems. Nanodiamond is used as a polishing material,[39] an additive in rubbers[40] and lubricants,[39] and in drug delivery and bioimaging.[41] Use of DNPs in the present study was motivated by their chemical stability and the ease with which they can be functionalized, allowing us to probe interactions with NOM and model and actual bacterial surfaces without complications arising from dissolution of the nanoparticle core material.[42] We chose the PAH polymer to functionalize the DNPs to investigate the impact of NOM on a capping agent previously shown to be toxic to bacteria and the microcrustacean *Daphnia magna* when mounted on nanogold.[43-44] We used quartz crystal microbalance with dissipation monitoring (QCM-D) to investigate nanoparticle interaction with model membranes lacking or incorporating LPS. We further examined the impact of NOM on membrane damage and toxicity to *S. oneidensis* induced

by PAH-DNP. The results presented here provide new insights into how NOM affects the interaction of nanomaterials with bacterial membranes.

MATERIALS AND METHODS

Functionalization of diamond nanoparticles. Diamond nanoparticles (Monocrystalline Synthetic Diamond, MSY 0-0.03 μm) were obtained from Microdiamant (Legwil, Switzerland). As-received DNPs were oxidized by reflux in a 3:1 (v/v) mixture of concentrated H_2SO_4 and HNO_3 for 3 d (Caution: extremely caustic). After oxidation the nanodiamond was diluted (10×) in ultrapure water (18.2 MΩ·cm resistivity, MilliQ-Advantage A10, Millipore) and centrifuged (5 min, 4696*g*) to sediment the particles. After an additional wash (centrifugation and resuspension in ultrapure water), the pellet was resuspended in 3:1 (v/v) H_2SO_4:HNO_3 and refluxed for another 3 d. The resulting nanoparticle suspension was diluted, centrifuged (5 min, 4696*g*), and resuspended repeatedly until the pH was neutral and the particles did not sediment. The dispersed particles were electrostatically wrapped with PAH polymer (15 kDa, Sigma Aldrich) by mixing particles (1 $mg \cdot mL^{-1}$ as determined by gravimetric analysis) with polymer solution (1 $mg \cdot mL^{-1}$ in 0.001 M NaCl) at a 1:1 ratio overnight. Particles were dialyzed (Spectrum Labs, nominal molecular weight cut-off 50 kDa) against 4 L of ultrapure water three times (4 h the first time and 24 hr each for the two subsequent times) to remove excess polymer.

Natural organic matter. Suwannee River NOM was obtained from the International Humic Substances Society (1R101N, St. Paul, MN). Stock solutions of NOM (200 $mg_{oc} \cdot L^{-1}$) were prepared in ultrapure water (18.2 MΩ·cm resistivity, Barnstead GenPure Pro) adjusted to pH 10 with 6 M NaOH. The solution was allowed to stir overnight in the dark, filtered through a 0.22 μm Teflon® filter, and stored at 4 °C. The total organic content in the stock solution was determined after filtration using the UV/persulfate oxidation method with membrane

conductometric detection of CO_2 (GE Instruments/Sievers Model 900 TOC analyzer, 186 ± 13 $mg_{oc} \cdot L^{-1}$). Prior to use in experiments, NOM solutions were buffered to pH 7.4 with 0.002 M 4-(2-hydroxyethyl)-1-piperazineethanesulfonic acid (HEPES, Fisher Scientific) and the ionic strength was adjusted to 0.025 M with NaCl.

Hydrodynamic and electrokinetic characterization. We determined diffusivities and electrophoretic mobilities of PAH-DNPs over a range of NOM-to-DNP concentration ratios, by dynamic light scattering and laser Doppler microelectrophoresis (75 V; Malvern ZetaSizer Nano ZS, Worcestershire, UK). Unless otherwise noted, experiments were conducted at a 1 nM number concentration of PAH-DNP in 0.025 M NaCl buffered to pH 7.4 with 0.002 M HEPES (ionic strength and pH values within the ranges encountered in natural freshwater systems).[45] After addition of PAH-DNP to a buffered NOM solution, the mixture was vortexed and analyzed immediately. (Experiments were conducted to evaluate the effect of contact time on DLS and ζ potential measurements, and we saw no significant differences between immediate analysis and analysis after 1 h of contact time, here we report findings for the case where the particles were mixed and immediately analyzed). Diffusivity and electrophoretic mobility measurements represent averages of five measurements. We calculated intensity-averaged hydrodynamic diameters from the particle diffusivities using the Stokes−Einstein equation. Hydrodynamic diameter (d_h) number distributions were estimated from the intensity measurements using Mie theory.[46] We estimated DNP ζ-potentials from the electrophoretic mobility using the Smoluchowski approximation.[47-48] The Smoluchowski approximation assumes the particle is a hard sphere; however, the polyelectrolyte coatings on the nanodiamond used here renders a relatively soft, ion-penetrable shell on a hard particle core, making the ζ-potential derived from the Smoluchowski approximation an apparent value.[48]

Quantification of free NOM in solution. Ultraviolet-visible (UV-Vis) absorption spectroscopy was used to determine the amount of chromophoric NOM bound to the surface of the PAH-DNPs (Shimadzu UV-2401PC). Samples varying in NOM-to-DNP ratio were prepared as described for DLS measurements and then centrifuged (90 min, 25,000*g*, 25 °C) to produce a pellet of either PAH-DNP or NOM/PAH-DNP. Supernatant was removed, and the chromophoric NOM remaining in the supernatant was quantified by comparing the absorbance at 320 nm to a calibration curve made from a stock NOM solution (Figure S1).

Preparation and characterization of phospholipid vesicles. We prepared small unilamellar vesicles (SUVs) composed of solely 1-palmitoyl-2-oleoyl-*sn*-glycero-3-phosphocholine (POPC, 16:0-18:1 PC; Avanti Polar Lipids) or with 0.46 mol% rough LPS (rLPS) or smooth LPS (sLPS) or 6.4 mol% rLPS as recently described.[33] Rough and smooth LPS were from *Salmonella enterica* serotype minnesota Re 595 (the so-called deep rough mutant) and serotype minnesota, respectively (Sigma Aldrich). Further details on preparation and characterization of these vesicles, as well as the generic structure of LPS are presented in the Supporting Information (Figures S2 and S3).

Interaction of diamond nanoparticles with supported lipid bilayers. We used QCM-D to monitor the formation of supported lipid bilayers and their interactions with nanoparticles in real time and without the use of labels. The QCM-D technique measures the changes in resonance frequency (Δf) and energy dissipation (ΔD) for an AT-cut quartz crystal as an analyte interacts with the sensor surface. Changes in frequency are related to changes in the mass coupled to the sensor surface, which includes the mass of both the analyte and of any dynamically coupled solvent. The dissipation factor, D, represents the fractional energy loss per radian at the oscillation frequency and provides information on the viscoelastic properties of

laterally homogeneous adlayers or the stiffness of particle–surface contacts for films of discrete nanosized objects.[49] Rigidly adsorbed films have a fractional energy loss per radian of oscillation that is small relative to the change in frequency of a given harmonic (n), defined $-\Delta D_n/(\Delta f_n/n) << 2/(f_n)$ (equal to 4×10^{-7} Hz^{-1} for the 4.96 MHz crystals used here),[49] where n is the harmonic number. For such films, the adsorbed surface mass density ($\Delta\Gamma_{QCM\text{-}D}$) is linearly related to the change in frequency, as described by the Sauerbrey equation:[50]

$$\Delta\Gamma_{QCM\text{-}D} = -\frac{C}{n}\Delta f_n \quad (2)$$

where C is the mass sensitivity constant (equal to 18.0 $ng \cdot Hz^{-1} \cdot cm^{-2}$ for a 4.96 MHz crystal). In the PAH-DNP experiments presented, $-\Delta D_n/(\Delta f_n/n) < 4 \times 10^{-7}$ Hz^{-1} (Table S7), and the Sauerbrey equation was used to estimate acoustic surface mass density. The fundamental and odd harmonics (n = 3-11) were measured simultaneously. Data from odd harmonics 3 through 11 were equivalent;[51] we present data from the 5th harmonic (~25 MHz) for all studies. Initial rates of PAH-DNP deposition (r_d) were calculated as the first derivative of the change in acoustic surface mass density with respect to time over the first 30 seconds of attachment:[52-54]

$$r_d = \frac{d\Gamma_{QCM\text{-}D}}{dt} \quad (3)$$

Prior to QCM-D experiments, SiO_2-coated sensor crystals (QSX303, Biolin Scientific, Stockholm, Sweden) were cleaned by sonicating in a 2% sodium dodecyl sulfate solution (10 min), rinsing alternatively with ultrapure water and ethanol three times, drying with N_2 gas, and exposed to ultraviolet light (185 nm and 254 nm) from a low-pressure mercury lamp (20 min) to remove any trace organic compounds (Bioforce Nanosciences UV/Ozone Procleaner).

We formed supported lipid bilayers on SiO_2-coated quartz crystal microbalance sensors from SUVs composed of POPC with or without LPS via the vesicle fusion method[33,38,55] using a

Q-Sense E4 instrument (Biolin Scientific). The sensors were first equilibrated in 0.150 M NaCl buffered to pH 7.4 with 0.002 M HEPES (pH and buffer concentration used throughout unless otherwise noted). Vesicles (0.125 $mg \cdot mL^{-1}$) in a solution of the same composition were flowed (0.100 $mL \cdot min^{-1}$) over the surface until the critical surface vesicle concentration (evidenced as the time at which the maximum frequency change is observed)[56] was attained and the vesicles ruptured and fused to form a bilayer. After frequency and dissipation values stabilized, vesicle-free solution was flowed over the sensor to remove any loosely adsorbed vesicles. The ionic strength was lowered by exchanging the 0.150 M NaCl solution with 0.025 M NaCl solution until a stable baseline was reached. Figure S4 shows a representative frequency trace.

Suspensions of PAH-DNP with or without NOM (5 or 30 $mg_{oc} \cdot L^{-1}$) or NOM alone (5 or 30 $mg_{oc} \cdot L^{-1}$) in 0.025 M NaCl were flowed over the supported lipid bilayers, and attachment was monitored for 20 min. (For samples including NOM and PAH-DNPs, PAH-DNPs were exposed to NOM for up to 20 min before introduction to the QCM-D as no further aggregation of the particles was observed by DLS in this time frame.) After 20 min, bilayers were rinsed with nanoparticle-free solution to examine the reversibility of attachment. In a subset of experiments, the bilayer was equilibrated with 4.7 $mg \cdot L^{-1}$ PAH polymer prior to the introduction of PAH-DNP (with or without NOM) to examine the influence of adsorbed polymer on nanoparticle attachment to the bilayers (Table S9). Attachment experiments were conducted in at least triplicate at 25.0 ± 0.5 °C.

***Shewanella oneidensis* viability and membrane damage.** *Shewanella oneidensis* was grown from colonies on an agar plate in *Difco*™ Luria-Bertani (LB) Broth overnight in a shaker incubator (30 °C, 275 rpm). Cells were sedimented (2000*g*, 10 min) and resuspended in Dulbecco's phosphate-buffered saline (D-PBS), and sedimented and resuspended

again in fresh 0.025 M NaCl buffered to pH 7.4 with 0.002 M HEPES before exposure to nanoparticles.

We evaluated the toxicity of PAH-DNP to *S. oneidensis* using a growth-based viability assay to quantify actively metabolizing cells.[57] The time for a cell culture to reach log phase depends on initial cell density: the longer the delay (lag phase), the lower the initial viable cell density (measured in colony forming units, CFU). A calibration curve of *S. oneidensis* was constructed using serially diluted cell culture where 10^7 CFU·mL^{-1} was defined as 100% viable. A *S. oneidensis* culture at 10^7 CFU·mL^{-1} was incubated (10 min) with NOM alone or with NOM+DNP at ratios ranging from 0 to 6.67 $mg_{oc} \cdot mg_{PAH\text{-}DNP}^{-1}$, then diluted in fresh LB medium in a 96-well plate. Optical density at 600 nm was monitored at 20-min intervals for 20 h (SpectraMax Plate Reader) at 30 °C with agitation between readings to track cell growth. The time to reach log phase for each exposure condition was compared to the calibration curve to determine any change in viability.

The LIVE/DEAD BacLight^{TM} kit (ThermoFisher Scientific) was used to assess bacterial membrane damage by PAH-DNP in the presence and absence of NOM. We exposed *S. oneidensis* to 1 nM PAH-DNP at NOM-to-DNP ratios ranging from 0 to 6.67 $mg_{oc} \cdot mg_{PAH\text{-}DNP}^{-1}$ for 10 min, and the cells were distributed in a 96-well plate in triplicate. The LIVE/DEAD stain mixture was used according to manufacturer recommendations. Analyses were conducted using a fluorescence plate reader using an excitation wavelength of 485 nm. Fluorescence intensity was measured at 528 nm and 635 nm for SYTO9 and propidium iodide (PI), respectively. SYTO9-to-PI fluorescence intensity ratios were determined for each exposure and normalized to that of a control bacterial sample not exposed to either PAH-DNP or NOM.

Statistical analyses. Comparisons across bilayer types and particle conditions were made using a two-way ANOVA with a Tukey correction for multiple comparisons at the $\alpha = 0.05$ level of significance (Prism 6.0).

RESULTS AND DISCUSSION

NOM alters nanoparticle hydrodynamic and electrokinetic properties. We determined the hydrodynamic diameter (d_h) and ζ-potential of the PAH-DNPs over a range of NOM concentrations (0 to 30 $mg_{oc} \cdot L^{-1}$) representing NOM-to-PAH-DNP ratios of 0 to 8 $mg_{oc} \cdot mg_{PAH\text{-}DNP}^{-1}$. Interaction with NOM induced changes to PAH-DNP d_h (Figure 1a) and ζ-potential (Figure 1b). In the absence of NOM at an ionic strength of 0.025 M and a pH of 7.4 (0.002 M HEPES), PAH-DNPs were present in suspension primarily as single positively charged nanoparticles ($d_h = 17 \pm 6$ nm, equivalent to the nominal core size of the nanoparticles, ~15 nm; ζ-potential = +21 ± 3 mV). At a NOM-to-DNP ratio of 1.33 $mg_{oc} \cdot mg_{PAH\text{-}DNP}^{-1}$, the d_h of PAH-DNP increased to 42 ± 9 nm, indicating a modest degree of aggregation, but the ζ-potential remained unchanged (+22.3 ± 0.6 mV). Measurement of the NOM in solution that was not bound to PAH-DNPs at this NOM-to-DNP ratio was thwarted by the inability to sediment these particles from suspension even at centrifugal forces up to 649,555*g* for 120 min. The PAH-DNPs were more stable with respect to sedimentation at 1.33 $mg_{oc} \cdot mg_{PAH\text{-}DNP}^{-1}$ than when no NOM was present. Increasing the NOM-to-DNP ratio to 2.67 $mg_{oc} \cdot mg_{PAH\text{-}DNP}^{-1}$ resulted in further particle aggregation and a reversal of ζ-potential to –13.0 ± 0.4 mV. At NOM-to-DNP ratios of 4 $mg_{oc} \cdot mg_{PAH\text{-}DNP}^{-1}$ and higher, the d_h and ζ-potentials of the PAH-DNP remained relatively constant, near 40 nm and –30 mV, respectively. Sedimentation of aggregates formed at NOM-to-DNP ratios of 2.67 and 8 $mg_{oc} \cdot mg_{PAH\text{-}DNP}^{-1}$ from suspension by centrifugation (90 min, 25,000*g*) and determination of

the amount of NOM remaining in the supernatant (Figure S1), suggested that 2.1 $mg_{oc} \cdot mg_{PAH\text{-}DNP}^{-1}$ bound to the surface of the DNP (0.011 $mg_{oc} \cdot nm^{-2}$).

We attribute the decrease in PAH-DNP ζ-potential with increasing NOM-to-DNP concentration ratio primarily to electrostatic interaction of deprotonated carboxyl groups of NOM with the positively charged pendant primary amines on the PAH polymers. At low NOM-to-DNP ratios (≤ 1.33 $mg_{oc} \cdot mg_{PAH\text{-}DNP}^{-1}$), interaction with NOM molecules induces a small degree of aggregation, but the NOM molecules are not present at high enough concentration to neutralize the overall charge of the PAH-DNPs or displace the PAH polymer wrapping. At this low NOM-to-DNP ratio, aggregation may be due to NOM adsorption leading to uneven charge distribution and a concomitant attractive contribution to the interaction energy.[58-59] Aggregation induced by oppositely charged patches on nanoparticle surfaces is not satisfactorily represented by classical Derjaguin–Landau–Verwey–Overbeek (DLVO) theory.[60] As the NOM-to-DNP ratio increased, electrostatic interaction with NOM molecules neutralized and then reversed the positive charge on the DNPs; when the magnitude of the ζ-potential was small, attractive van der Waals forces overcame electrostatic repulsion between particles and destabilized the particle suspensions. Alternatively, aggregation rates may have risen as the probability of favorable interactions increased between oppositely charged regions on the DNP surfaces (a function of surface coverage and charge density of both the PAH and the adsorbing NOM molecules) leading to maximum aggregation rates at non-zero net surface charge.[58-59] At yet higher NOM-to-DNP ratios (≥4 $mg_{oc} \cdot mg_{PAH\text{-}DNP}^{-1}$), the NOM-coated particles possessed strongly negative ζ-potentials (–30 mV) and yielded stable suspensions of DNP aggregates with comparable d_h (one-way ANOVA, $p = 0.2334$). The observed charge reversal indicated that NOM molecules either overcoat the positively charged polymer on the nanodiamond surface, forming a "NOM corona"

around the particles, or displaced the electrostatically wrapped PAH polymer. Charge reversal of positively charged bare zinc oxide,[61-62] hematite,[15] and titanium dioxide[16] due to interaction with NOM has been reported previously. Furthermore, increasing the concentration ratio of NOM to gold nanoparticles functionalized with positively charged branched polyethylenimine or aminated polyethylene glycol led to charge neutralization and ultimately charge reversal much like we observed with PAH-DNPs.[17] Our findings are consistent with these results and demonstrate the same phenomenon for particles differing in core material and initial organic coating.

Nanodiamond attachment to zwitterionic phospholipid bilayers. We next investigated the impact of the NOM-induced changes to PAH-DNP properties on their interaction with model membranes composed of the zwitterionic phospholipid POPC. We examined the influence of NOM on initial attachment rates to and acoustic surface mass densities attained on POPC bilayers of PAH-DNPs at NOM-to-DNP ratios of 0, 1.33, and 8 $mg_{oc} \cdot mg_{PAH\text{-}DNP}^{-1}$ by QCM-D (Figure 2). Consistent with expectations, electrostatic attraction between the positively charged PAH-DNP and the negative potential of the supported zwitterionic POPC bilayer[34,63] led to attachment in the absence of NOM (Figure 2). We calculated the efficiency of PAH-DNP attachment to lipid bilayers to quantify the kinetics of initial attachment:[64]

$$\alpha_D = \frac{\left(d\Gamma_{QCM\text{-}D}/dt\right)_{\text{lipid bilayer}}}{\left(d\Gamma_{QCM\text{-}D}/dt\right)_{fav}} \qquad (5)$$

where $d\Gamma_{QCM\text{-}D}/dt$ is the change in adsorbed surface mass density per unit time and the subscript fav on the term in the denominator refers to the change in adsorbed surface mass density under favorable deposition conditions (absence of an energy barrier to deposition). In the present study, we approximated favorable deposition conditions for the positively charged PAH-DNPs using

the strongly negatively charged SiO_2 surface.[63] To do this, we empirically determined initial rates of attachment to SiO_2 under the same conditions used for the bilayers. We found all attachment efficiencies for PAH-DNPs to be near unity (Table S2), consistent with previous findings of favorable interaction between cationic nanoparticles and zwitterionic lipid bilayers.[33,65-66] We hypothesize that the amine groups on the PAH polymer on the nanodiamond interacted with the phosphate group in the phosphatidylcholine headgroup of the POPC lipids.[67-68] The surface mass density of PAH-DNPs attained after 20 min was higher on the POPC bilayer than on SiO_2 by a factor of ~3.6 (Figure 2b, Table S8). Lateral repulsion between positively charged PAH-DNP appears to limit the extent of attachment on the SiO_2 surface. Lateral repulsion seems to be diminished on the POPC bilayer, likely due to phospholipid extraction,[35,67] allowing higher surface densities to be reached. Rinsing with nanoparticle-free solution produced small (9 ± 2 ng·cm^{-2}) decreases in acoustic mass consistent with removal of a small population of loosely adhered PAH-DNPs. The attachment of the remaining PAH-DNPs was irreversible on the timescale of our experiments.

At the low NOM-to-DNP ratio of 1.33 $mg_{oc} \cdot mg_{PAH\text{-}DNP}^{-1}$, the PAH-DNP aggregated to a moderate extent ($d_h = 42 \pm 9$ nm) and retained a positive ζ-potential ($+22.3 \pm 0.6$ mV). The initial rate of PAH-DNP attachment to POPC bilayers at this low NOM-to-DNP ratio did not differ significantly from that for PAH-DNP in the absence of NOM ($p > 0.05$; Figure 2a and Table S1), and attachment efficiencies were close to unity (Table S2). This result is not attributable to the deposition of NOM itself to the bilayer. Control experiments showed the initial rate of NOM attachment to POPC to be nearly zero at a concentration of 5 $mg_{oc} \cdot L^{-1}$ (the total NOM concentration in the 1.33 $mg_{oc} \cdot mg_{PAH\text{-}DNP}^{-1}$ NOM-to-DNP suspensions; Table S1). Furthermore, exposure of POPC bilayers to 5 $mg_{oc} \cdot L^{-1}$ NOM prior to introduction of PAH-DNP did not alter

the initial attachment rate (–1.8 ± 0.2 ng·cm^{-2}·s^{-1}; $p > 0.05$). We expect transport of the aggregates formed in the presence of 5 mg_{oc}·L^{-1} NOM to the model membrane surface to be slower than that of the individual PAH-DNPs. Using a Lévêque solution for convective-diffusive transport modified to account for the curvilinear flow in the QCM-D flow chamber,[69] we estimate that in the presence of 5 mg_{oc}·L^{-1} NOM the spatially averaged mass-transport limited attachment rate constant is smaller by a factor of 0.56 ± 0.15 relative to the case without NOM (for details of this analysis see the Supporting Information). The equivalence of the initial attachment rates in the absence and presence of 5 mg_{oc}·L^{-1} NOM implies that the average effective mass of the aggregates (mass of PAH-DNPs, NOM and internal water) attaching to the model membrane during the initial attachment period is roughly twice that of the individual PAH-DNPs.

The acoustic surface mass density (Γ_{QCM-D}) of PAH-DNP on POPC bilayers after 20 min exposure under flowing conditions was substantially larger at a NOM-to-DNP ratio of 1.33 mg_{oc}·$mg_{PAH-DNP}^{-1}$ than in the absence of NOM ($p < 0.0001$; Figure 2b, Table S8) and was accompanied by larger energy dissipation than in the absence of NOM (Table S6) and more pronounced dispersion in $\Delta f_n/n$ indicating that the NOM/PAH-DNP aggregates were less rigidly coupled to the oscillating sensor than in the absence of NOM. Rinsing with PAH-DNP- and NOM-free solution resulted in no net change in acoustic mass indicating that NOM/PAH-DNP attachment to POPC bilayers was irreversible over experimental time scales. The much larger Γ_{QCM-D} was not attributable to adsorption of NOM alone; exposure of POPC bilayers to 5 mg_{oc}·L^{-1} NOM in the absence of PAH-DNP resulted in Γ_{QCM-D} values far too small (Table S8) to account for the large difference observed in PAH-DNP attachment in the presence and absence of this concentration of NOM. Furthermore, Γ_{QCM-D} for attachment to POPC bilayers was statistically

indistinguishable whether or not the bilayers had been first exposed to 5 $mg_{oc} \cdot L^{-1}$ NOM for 20 min prior to interaction with PAH-DNP. We therefore attributed the higher $\Gamma_{QCM\text{-}D}$ at the 1.33 $mg_{oc} \cdot mg_{PAH\text{-}DNP}^{-1}$ NOM-to-DNP ratio relative to that in the absence of NOM to NOM-induced changes to PAH-DNP properties. As noted above, adsorption of NOM molecules may lead to electrostatic attraction between oppositely charged regions on adjacent DNPs and thereby a moderate degree of aggregation at NOM concentrations insufficient to induce rapid aggregation while the ζ-potential remains positive. The effective mass of these aggregates (mass of PAH-DNPs, NOM and internal water) is higher than that of single PAH-DNPs. We therefore attributed the higher $\Gamma_{QCM\text{-}D}$ at a NOM-to-DNP ratio of 1.33 $mg_{oc} \cdot mg_{PAH\text{-}DNP}^{-1}$ to the larger effective mass of the aggregated particles delivered to the sensor surface.

At a NOM-to-DNP ratio of 8 $mg_{oc} \cdot mg_{PAH\text{-}DNP}^{-1}$, NOM molecules induced a modest degree of aggregation (d_h = 34 ± 13 nm) and coated the PAH-DNPs to the extent that the surface charge was reversed and the ζ-potential was strongly negative (–33 ± 1 mV). At this NOM-to-DNP ratio, the initial rate of PAH-DNP deposition was more than an order of magnitude lower than in the absence of NOM ($p < 0.0001$; Figure 2a, Table S1) and $\Gamma_{QCM\text{-}D}$ values at 20 min were much smaller than in the absence of NOM (Figure 2b, Table S8). The NOM concentration remaining in PAH-DNP suspensions at the NOM-to-DNP ratio used here was ~22 $mg_{oc} \cdot L^{-1}$. We examined the initial rate of deposition of 30 $mg_{oc} \cdot L^{-1}$ NOM (the total NOM concentration in the 8 $mg_{oc} \cdot mg_{PAH\text{-}DNP}^{-1}$ NOM-to-DNP suspensions) and the adsorbed surface mass density at 20 min and found the NOM deposition rate and $\Gamma_{QCM\text{-}D}$ to be comparable to those measured for the 8 $mg_{oc} \cdot mg_{PAH\text{-}DNP}^{-1}$ NOM-DNP ratio (Figure 2b, Table S1). We therefore attribute the small frequency shifts observed in the NOM-DNP attachment experiments at the high NOM-to-DNP ratio to NOM molecules adsorbing to the bilayer. These results are consistent with following

interpretation: NOM molecules overcoated the PAH-DNP or displaced the electrostatically wrapped PAH polymer on the DNP surface to the extent that the ζ-potential of the aggregates became strongly negative resulting in a significant electrostatic energy barrier to attachment to the negatively charged supported model membranes to which NOM had adsorbed.[65,70]

Nanodiamond interaction with phospholipid bilayers containing lipopolysaccharides. Full-length, or smooth, LPS is composed of three parts: Lipid A, a core oligosaccharide, and an *O*-polysaccharide (Figure S2).[71-73] The presence or absence of an *O*-polysaccharide determines whether a LPS molecule is respectively smooth or rough.[71] Rough LPS (expressed by some bacteria) is a truncated form of LPS, which contains Lipid A and at least part of the core oligosaccharide, but lacks the outer *O*-polysaccharide. The rough LPS produced by deep rough mutant 595 used in the present study is composed of Lipid A and two residues of 2-keto-3-deoxy-D-manno-octonate (Kdo) in the core oligosaccharide. In contrast, the smooth LPS also contained a variable length O-polysaccharide lacking acidic residues and the portion of the core oligosaccharide between the Kdo residues and the O-polysaccharide, which includes two phosphate groups.[33,74] The core oligosaccharide of the deep rough and smooth LPS thus contained two and four negative charges, respectively.

Due to the relevance and abundance of these biomolecules at Gram-negative bacterial surfaces we investigated the effect of including rough or smooth LPS molecules in supported POPC bilayers on PAH-DNP interaction with model membranes in the absence and presence of NOM. To construct bilayers incorporating LPS, we employed the vesicle fusion method using LPS-containing POPC vesicles. Vesicles incorporating LPS exhibited more negative ζ-potentials than did those composed solely of POPC (Figure S3). Smooth LPS is larger and more negatively charged than is deep rough LPS. Electrostatic and steric repulsion limits the maximum amount of

smooth LPS that can be incorporated into SiO_2-supported model membranes via the vesicle fusion method to a lower mol% than can be achieved with rough LPS.[33,38] To enable direct comparison between the two types of LPS we therefore prepared bilayers from vesicles containing 0.46 mol% rough or smooth LPS. To examine the impact of rough LPS surface density on PAH-DNP attachment, we also formed bilayers from vesicles containing 6.4 mol% rLPS.

Initial rates of PAH-DNP attachment to POPC bilayers and those formed from vesicles containing 0.46 mol% rLPS or sLPS were statistically indistinguishable ($p > 0.05$; Figure 2a, Table S1) and attachment efficiencies were close to 1 (Table S2). This is likely attributable to the small amount of LPS incorporated into these membranes. Increasing vesicle rLPS content from 0.46 to 6.4 mol% produced a small decrease in the initial rate of PAH-DNP attachment relative to that of POPC ($p < 0.01$, Figure 2a, Table S1). Increasing the incorporation of rough LPS into vesicles by a factor of ~14 decreased the ζ-potential of the vesicles from –12.6 ± 3.6 mV to –41.7 ± 2.2 mV(Figure S3). We therefore hypothesize that the decrease in r_d was due to the LPS groups sterically hindering accessibility to the negative charges on the phosphatidylcholine groups of the bilayer. Values for $\Gamma_{QCM\text{-}D}$ after 20 min attachment of PAH-DNPs to POPC bilayers and those incorporating rLPS or sLPS were statistically indistinguishable ($p > 0.05$; Figure 2b, Table S8).

At a low NOM-to-DNP ratio of 1.33 $mg_{oc} \cdot mg_{PAH\text{-}DNP}^{-1}$, the initial rates and attachment efficiencies of NOM/PAH-DNPs attachment to bilayers containing 0.46 mol% rough or smooth LPS were equal to those measured in the absence of NOM ($p > 0.05$; Figure 2a, Table S1). Equivalent amounts of NOM at this ratio (5 $mg_{oc} \cdot L^{-1}$) showed little attachment to 0.46 mol% rLPS and no attachment to 0.46 mol% smooth or 6.4 mol% rough LPS. In the case of 6.4 mol%

rLPS, an increase in attachment rate was observed relative to that in the absence of NOM (p <0.0001). Acoustic surface mass densities after 20 min attachment of NOM/PAH-DNPs to all bilayers were higher at a NOM-to-DNP ratio of 1.33 $mg_{oc} \cdot mg_{PAH\text{-}DNP}^{-1}$ relative to those obtained in the absence of NOM ($p < 0.0001$; Figure 2b, Table S8). As noted in the case of POPC, the larger $\Gamma_{QCM\text{-}D}$ values may be attributable to the higher mass associated with the aggregated particles (PAH-DNPs, NOM and internal water) at this NOM-to-DNP ratio.

As we observed for POPC bilayers for NOM-to-DNP ratios of 8 $mg_{oc} \cdot mg_{PAH\text{-}DNP}^{-1}$, attachment rates to bilayers containing LPS were at least an order of magnitude lower than in the absence of NOM and indistinguishable from one another (Figure 2a, Table S1). The deposition rate of 30 $mg_{oc} \cdot L^{-1}$ NOM with no PAH-DNP (the total NOM concentration in the 8 $mg_{oc} \cdot mg_{PAH\text{-}DNP}^{-1}$ NOM-to-DNP suspensions) was similar to that observed when particles were present to all three bilayer types (Table S1). Furthermore, the acoustic surface mass density of the 8 $mg_{oc} \cdot mg_{PAH\text{-}DNP}^{-1}$ particles after 20 min attachment was indistinguishable from that of NOM binding to the bilayer (Table S8, $p > 0.05$). Therefore, we attribute the observed attachment rate and attachment for the 8 $mg_{oc} \cdot mg_{PAH\text{-}DNP}^{-1}$ particles solely to NOM binding to the 0.46 mol% rLPS and 0.46 mol% sLPS bilayers. Neither attachment of particles at NOM-to-DNP ratios of 8 $mg_{oc} \cdot mg_{PAH\text{-}DNP}^{-1}$ nor NOM itself was observed to attach to the 6.4 mol% rLPS bilayer likely due to increased electrostatic repulsion between the NOM and the more negatively charged bilayer relative to the other three studied here (Figure S3).

Natural organic matter modulates PAH-DNP impact on *Shewanella oneidensis*. We examined the influence of NOM on the effect of PAH-DNP on the Gram-negative bacterium *Shewanella oneidensis*. A significantly higher coverage of LPS was expected on bacterial surfaces (up to 75%) than was modeled in the membrane studies; nonetheless, we

anticipated a similar trend in surface attachment to bacterial cells to be observed. We note that under the growth conditions in this study (30 °C), *S. oneidensis* elaborates only rough LPS.[33]

We employed the LIVE/DEAD assay to quantify membrane damage. This fluorescence-based method uses two fluorescent dyes that bind to nucleic acid: green-fluorescent SYTO 9 and red-fluorescent PI. Cell-permeant SYTO 9 stains all live cells; the non-permeant PI stains nucleic acids only in the cells with damaged membranes. In the absence of NOM, exposure to 1 nM PAH-DNP resulted in membrane damage to >60% of the cells (Figure 3a). As the NOM-to-DNP ratio increased, the proportion of cells with membrane damage remained unchanged at ratios up to 0.8 $mg_{oc} \cdot mg_{PAH\text{-}DNP}^{-1}$. A sharp increase in the proportion of cells with intact membranes was observed at ratios between 0.8 and 1.1 $mg_{oc} \cdot mg_{PAH\text{-}DNP}^{-1}$, with no observable damage above a ratio of 1.1 $mg_{oc} \cdot mg_{PAH\text{-}DNP}^{-1}$.

The impact of NOM on the toxicity to *S. oneidensis* induced by exposure to PAH-DNP exhibited a similar trend (Figure 3b). The toxicity of 1 nM PAH-DNP was completely ameliorated at NOM-to-DNP ratios $\geq$ 1.3 $mg_{oc} \cdot mg_{PAH\text{-}DNP}^{-1}$. The strong correspondence between the membrane damage and bacterial viability results displayed in Figure 3 was expected. Earlier studies have indicated that the toxicity of cationic polymer-wrapped nanoparticles arises largely from attachment of the positively charged particles to negatively charged bacterial surfaces leading to membrane damage.[44] The reduced toxicity and membrane damage at higher NOM-to-DNP ratios are consistent with the drastically reduced attachment of PAH-DNP to supported bilayers containing 6.4% rough LPS at NOM-to-DNP ratios of 8 $mg_{oc} \cdot mg_{PAH\text{-}DNP}^{-1}$ (Figure 2b). The discrepancy between the results obtained at 1.3 $mg_{oc} \cdot mg_{PAH\text{-}DNP}^{-1}$ in the whole cell and 6.4% rLPS-POPC studies may be attributable to the much higher LPS content on cell surfaces. The higher density of rLPS on the bacterial surface may have sterically hindered nanoparticle

disruption of the outer membrane. We also note that the critical NOM-to-DNP ratio that resulted in amelioration in toxicity and membrane damage by PAH-DNP occurred at a slightly lower NOM-to-DNP ratio than that of charge reversal of the nanoparticle by NOM (Figure 1b). An earlier study examining the attachment to and uptake by HeLa cells of an array of Au nanoparticles spanning a range of ζ-potentials found a threshold of effective surface charge density below which minimal binding occurred even when the particles exhibited positive ζ-potentials.[75] Our observations likely reflect such a threshold in effective charge density as modulated by adsorbed NOM molecules.

Environmental implications. We have demonstrated that hydrodynamic and electrokinetic properties of DNPs wrapped with the polycation PAH are altered upon interaction with NOM and that NOM influences the interaction of these nanoparticles with model cell membranes and with intact bacterial cells. As the NOM-to-DNP ratio increased the following sequence of events occurred. Initial adsorption of NOM molecules to PAH-DNP surfaces resulted in uneven charge distributions and induced attractive interactions between oppositely charged regions on adjacent particles leading to a moderate degree of aggregation. As further NOM molecules adsorbed to DNP surfaces, the probability of favorable interactions between oppositely charged regions on the DNP surfaces increased leading to higher aggregation rates. Concurrently, adsorbing NOM molecules progressively neutralized and eventually reversed the positive potential of the particles. Aggregation was promoted at NOM-to-DNP ratios producing low ζ-potentials because the electrostatic energy barrier had been lowered sufficiently to allow attractive van der Waals interactions to cause aggregation. At still higher NOM-to-DNP ratios, the amount of NOM on the particles increased and electrostatic repulsion prevented further aggregation of PAH-DNPs. The changes to PAH-DNP hydrodynamic and electrokinetic

properties influenced the attachment of these particles to model membranes and their toxicity toward a Gram-negative bacterium. Our results lead to the expectation that the influence of NOM on nanoparticle-induced effects depends on the NOM-to-nanoparticle ratio (as well as the affinity of NOM for the nanoparticle surface).

In the experiments described here, a finite amount of NOM was available to bind to the PAH-DNP. This is particularly important for the low NOM-to-DNP ratios studied because this imposes a limit on the extent of overcoating/displacement of PAH polymer in the experimental system. In the environment, the amount (mass) of NOM ultimately available would be large enough to eventually overcoat/displace the PAH polymer entirely, even at low NOM concentration. The concentration ratios of NOM to PAH-DNP studied here varied from 1.33 (for 5 $mg_{oc} \cdot L^{-1}$ NOM) to 8.0 (for 30 $mg_{oc} \cdot L^{-1}$ NOM). In typical freshwater environments the ratio of NOM to engineered nanoparticle is expected to be much larger due to the expected low concentrations of engineered nanoparticles.[17] Overcoating/displacement would occur, but more slowly at low NOM concentrations. Differences in kinetics of overcoating/displacement could have biological consequences, similar to those demonstrated here at different NOM concentrations, depending on how rapidly the nanoparticles come in contact with organismal surfaces.

The present study represents an initial demonstration of the complex influence that NOM can have on nanomaterial interactions with bacterial surfaces. The present study focused on a single type of nanoparticle (diamond) functionalized with a single capping agent (the cationic polymer poly(allylamine HCl)). In the specific system investigated, at low NOM-to-PAH-DNP ratios PAH-DNP bound to model membranes and elicited membrane damage in the bacteria. Higher ratios, which caused reversal of the charge of the polymer-wrapped nanodiamond,

reduced attachment to the model membranes and damage to bacterial membranes. Effects similar to those we observed at high NOM concentrations have been reported for nanoscale zero-valent iron to *Escherichia coli*,[29] although the mechanism of toxicity likely differed. We expect our results to be most directly transferable to positively charged natural colloids and engineered nanoparticles functionalized with cationic polymers[17,35] and ligands[14,35,76-77]. We hypothesize that NOM overcoating/replacement of ligands occurs at the high NOM-to-nanoparticle ratios expected in the environment; in environments with low NOM concentrations, this would occur at slower rates than observed in the present study. Future studies are needed to understand the influence of NOM properties and divalent cations on nanomaterial interactions with cell surfaces in the presence of NOM.

ASSOCIATED CONTENT

Supporting Information

Quantification of NOM; chemical structures of POPC, LPS, and PAH polymer; hydrodynamic and electrokinetic properties of vesicles; supplemental tables and materials and methods. This material is available free of charge via the Internet at http://pubs.acs.org.

AUTHOR INFORMATION

Corresponding Author

*Phone: 608-263-4971; e-mail: joelpedersen@wisc.edu

Present Addresses

[a] Adamás Nanotechnologies, Inc., PO Box 90696, Raleigh, NC 27675

Notes

The authors declare no competing financial interest.

ACKNOWLEDGMENTS

This work was supported by the NSF under the Center for Sustainable Nanotechnology, CHE-1503408. JK acknowledges financial support from the Lindstrom Fund through Augsburg College. We thank Tian (Autumn) Qiu for measuring the concentration of free PAH in solution, Joseph Buchman for collecting TEM images, and Rachel Abbott for assistance with DLS and laser Doppler electrophoresis measurements. The constructive comments of three anonymous reviewers are gratefully acknowledged.

REFERENCES

1. Nel, A.; Xia, T.; Madler, L.; Li, N. Toxic potential of materials at the nanolevel. *Science,* **2006,** *311,* 622-627.
2. Maurer-Jones, M. A.; Gunsolus, I. L.; Murphy, C. J.; Haynes, C. L. Toxicity of engineered nanoparticles in the environment. *Anal. Chem.,* **2013,** *85,* 3036-3049.
3. Mudunkotuwa, I. A.; Grassian, V. H. The devil is in the details (or the surface): Impact of surface structure and surface energetics on understanding the behavior of nanomaterials in the environment. *J. Environ. Monit.,* **2011,** *13,* 1135-1144.
4. Lundqvist, M.; Stigler, J.; Elia, G.; Lynch, I.; Cedervall, T.; Dawson, K. A. Nanoparticle size and surface properties determine the protein corona with possible implications for biological impacts. *Proc. Natl. Acad. Sci. U.S.A.,* **2008,** *105,* 14265-14270.
5. Sani-Kast, N.; Labille, J.; Ollivier, P.; Slomberg, D.; Hungerbuhler, K.; Scheringer, M. A network perspective reveals decreasing material diversity in studies on nanoparticle interactions with dissolved organic matter. *Proc. Natl. Acad. Sci. U.S.A.,* **2017,** *114,* 1756.
6. Sutton, R.; Sposito, G. Molecular structure in soil humic substances: The new view. *Environ. Sci. Technol.,* **2005,** *29,* 9009-9015.
7. Thurman, E. M., *Organic geochemistry of natural waters*. Martinus Nijhoff/Dr. W. Junk Publishers: Dordrecht, 1985.
8. Jones, M. N.; Bryan, N. D. Colloidal properties of humic substances. *Adv. Colloid Interface Sci.,* **1998,** *78,* 1-48.
9. Ritchie, J. D.; Perdue, E. M. Proton-binding study of standard and reference fulvic acids, humic acids, and natural organic matter. *Geochim. Cosmochim. Acta,* **2003,** *67,* 85-96.
10. Louie, S. M.; Tilton, R. D.; Lowry, G. V. Critical review: Impacts of macromolecular coatings on critical physicochemical processes controlling environmental fate of nanomaterials. *Environ. Sci.: Nano,* **2016,** *3,* 283-310.
11. Peijnenburg, W. J. G. M.; Baalousha, M.; Chen, J.; Chaudry, Q.; Von der kammer, F.; Kuhlbusch, T. A. J.; Lead, J.; Nickel, C.; Quik, J. T. K.; Renker, M.; Wang, Z.; Koelmans, A. A. A review of the properties and processes determining the fate of engineered nanomaterials in the aquatic environment. *Crit. Rev. Env. Sci. Technol.,* **2015,** *45,* 2084-2134.

12. Grillo, R.; Rosa, A. H.; Fraceto, L. F. Engineered nanoparticles and organic matter: A review of the state-of-the-art. *Chemosphere,* **2015,** *119,* 608-619.
13. Philippe, A.; Schaumann, G. E. Interactions of dissolved organic matter with natural and engineered inorganic colloids: A review. *Environ. Sci. Technol.,* **2014,** *48,* 8946-8962.
14. Stankus, D. P.; Lohse, S. E.; Hutchison, J. E.; Nason, J. A. Interactions between natural organic matter and gold nanoparticles stabilized with different organic capping agents. *Environ. Sci. Technol.,* **2011,** *45,* 3238-3244.
15. Kretzschmar, R.; Sticher, H. Transport of humic-coated iron oxide colloids in a sandy soil: Influence of Ca^{2+} and trace metals. *Environ. Sci. Technol.,* **1997,** *31,* 3497-3504.
16. Loosli, F.; Le Coustumer, P.; Stoll, S. TiO_2 nanoparticles aggregation and disaggregation in presence of alginate and Suwannee River humic acids. pH and concentration effects on nanoparticle stability. *Water Res.,* **2013,** *47,* 6052-6063.
17. Surette, M. C.; Nason, J. A. Effects of surface coating character and interactions with natural organic matter on the colloidal stability of gold nanoparticles. *Environ. Sci.: Nano,* **2016,** *3,* 1144-1152.
18. Lau, B. L. T.; Hockaday, W. C.; Ikuma, K.; Furman, O.; Decho, A. W. A preliminary assessment of the interactions between the capping agents of silver nanoparticles and environmental organics. *Colloids Surf., A,* **2013,** *435,* 22-27.
19. Zhang, W.; Rattanaudompol, U.; Li, H.; Bouchard, D. Effects of humic and fulvic acids on aggregation of aqu/nC_{60} nanoparticles. *Water Res.,* **2013,** *47,* 1793-1802.
20. Erhayem, M.; Sohn, M. Stability studies for titanium dioxide nanoparticles upon adsorption of Suwannee River humic and fulvic acids and natural organic matter. *Sci. Total Environ.,* **2014,** *468-469,* 249-257.
21. Furman, O.; Usenko, S.; Lau, B. L. Relative importance of the humic and fulvic fractions of natural organic matter in the aggregation and deposition of silver nanoparticles. *Environ. Sci. Technol.,* **2013,** *47,* 1349-1356.
22. Louie, S. M.; Tilton, R. D.; Lowry, G. V. Effects of molecular weight distribution and chemical properties of natural organic matter on gold nanoparticle aggregation. *Environ. Sci. Technol.,* **2013,** *47,* 4245-4254.
23. Louie, S. M.; Spielman-Sun, E. R.; Small, M. J.; Tilton, R. D.; Lowry, G. V. Correlation of the physicochemical properties of natural organic matter samples from different sources to their effects on gold nanoparticle aggregation in monovalent electrolyte. *Environ. Sci. Technol.,* **2015,** *49,* 2188-2198.
24. Gunsolus, I. L.; Mousavi, M. P.; Hussein, K.; Buhlmann, P.; Haynes, C. L. Effects of humic and fulvic acids on silver nanoparticle stability, dissolution, and toxicity. *Environ. Sci. Technol.,* **2015,** *49,* 8078-8086.
25. Yin, Y.; Shen, M.; Tan, Z.; Yu, S.; Liu, J.; Jiang, G. Particle coating-dependent interaction of molecular weight fractionated natural organic matter: Impacts on the aggregation of silver nanoparticles. *Environ. Sci. Technol.,* **2015,** *49,* 6581-6589.
26. Nason, J. A.; McDowell, S. A.; Callahan, T. W. Effects of natural organic matter type and concentration on the aggregation of citrate-stabilized gold nanoparticles. *J. Environ. Monit.,* **2012,** *14,* 1885-1892.
27. Liu, J.; Legros, S.; von der Kammer, F.; Hofmann, T. Natural organic matter concentration and hydrochemistry influence aggregation kinetics of functionalized engineered nanoparticles. *Environ. Sci. Technol.,* **2013,** *47,* 4113-4120.

28. Ha, Y.; Wang, X.; Liljestrand, H. M.; Maynard, J. A.; Katz, L. E. Bioavailability of fullerene under environmentally relevant conditions: Effects of humic acid and fetal bovine serum on accumulation in lipid bilayers and cellular uptake. *Environ. Sci. Technol.,* **2016,** *50,* 6717-6727.
29. Li, Z.; Greden, K.; Alvarez, P. J. J.; Gregory, K. B.; Lowry, G. V. Adsorbed polymer and NOM limits adhesion and toxicity of nano scale zerovalent iron to *E. coli*. *Environ. Sci. Technol.,* **2010,** *44,* 3462-3467.
30. Chen, K. L.; Bothun, G. D. Nanoparticles meet cell membranes: Probing nonspecific interactions using model membranes. *Environ. Sci. Technol.,* **2014,** *48,* 873-880.
31. Liu, X.; Chen, K. L. Interactions of graphene oxide with model cell membranes: Probing nanoparticle attachment and lipid bilayer disruption. *Langmuir,* **2015,** *31,* 12076-12086.
32. Rascol, E.; Devoisselle, J. M.; Chopineau, J. The relevance of membrane models to understand nanoparticles-cell membrane interactions. *Nanoscale,* **2016,** *8,* 4780-4798.
33. Jacobson, K. H.; Gunsolus, I. L.; Kuech, T. R.; Troiano, J. M.; Melby, E. S.; Lohse, S. E.; Hu, D.; Chrisler, W. B.; Murphy, C. J.; Orr, G.; Geiger, F. M.; Haynes, C. L.; Pedersen, J. A. Lipopolysaccharide density and structure govern the extent and distance of nanoparticle interaction with actual and model bacterial outer membranes. *Environ. Sci. Technol.,* **2015,** *49,* 10642-10650.
34. Troiano, J. M.; Olenick, L. L.; Kuech, T. R.; Melby, E. S.; Hu, D.; Lohse, S. E.; Mensch, A. C.; Dogangun, M.; Vartanian, A. M.; Torelli, M. D.; Ehimiaghe, E.; Walter, S. R.; Fu, L.; Anderton, C. R.; Zhu, Z.; Wang, H.; Orr, G.; Murphy, C. J.; Hamers, R. J.; Pedersen, J. A.; Geiger, F. M. Direct probes of 4 nm diameter gold nanoparticles interacting with supported lipid bilayers. *J. Phys. Chem. C,* **2015,** *119,* 534-546.
35. Leroueil, P. R.; Berry, S. A.; Duthie, K.; Han, G.; Rotello, V. M.; McNerny, D. Q.; Jr., J. R. B.; Orr, B. G.; Holl, M. M. B. Wide varieties of cationic nanoparticles induce defects in supported lipid bilayers. *Nano Lett.,* **2008,** *8,* 420-424.
36. Melby, E. S.; Mensch, A. C.; Lohse, S. E.; Hu, D.; Orr, G.; Murphy, C. J.; Hamers, R. J.; Pedersen, J. A. Formation of supported lipid bilayers containing phase-segregated domains and their interaction with gold nanoparticles. *Environ. Sci.: Nano,* **2016,** *3,* 45-55.
37. Le Brun, A. P.; Clifton, L. A.; Halbert, C. E.; Lin, B.; Meron, M.; Holden, P. J.; Lakey, J. H.; Holt, S. A. Structural characterization of a model Gram-negative bacterial surface using lipopolysaccharides from rough strains of *Escherichia coli*. *Biomacromolecules,* **2013,** *14,* 2014-2022.
38. Kaufmann, S.; Ilg, K.; Mashaghi, A.; Textor, M.; Priem, B.; Aebi, M.; Reimhult, E. Supported lipopolysaccharide bilayers. *Langmuir,* **2012,** *28,* 12199-12208.
39. Krueger, A. Diamond nanoparticles: Jewels for chemistry and physics. *Adv. Mater.,* **2008,** *20,* 2445-2449.
40. Shakun, A.; Vuorinen, J.; Hoikkanen, M.; Poikelispää, M.; Das, A. Hard nanodiamonds in soft rubbers: Past, present and future – a review. *Composites Part A: Applied Science and Manufacturing,* **2014,** *64,* 49-69.
41. Mochalin, V. N.; Shenderova, O.; Ho, D.; Gogotsi, Y. The properties and applications of nanodiamonds. *Nat. Nanotechnol.,* **2011,** *7,* 11-23.
42. Stavis, C.; Clare, T. L.; Butler, J. E.; Radadia, A. D.; Carr, R.; Zeng, H.; King, W. P.; Carlisle, J. A.; Aksimentiev, A.; Bashir, R.; Hamers, R. J. Surface functionalization of thin-film diamond for highly stable and selective biological interfaces. *Proc. Natl. Acad. Sci. U.S.A.,* **2011,** *108,* 983-988.

43. Bozich, J. S.; Lohse, S. E.; Torelli, M. D.; Murphy, C. J.; Hamers, R. J.; Klaper, R. D. Surface chemistry, charge and ligand type impact the toxicity of gold nanoparticles to *Daphnia magna*. *Environ. Sci.: Nano,* **2014,** *1,* 260-270.

44. Feng, Z. V.; Gunsolus, I. L.; Qiu, T. A.; Hurley, K. R.; Nyberg, L. H.; Frew, H.; Johnson, K. P.; Vartanian, A. M.; Jacob, L. M.; Lohse, S. E.; Torelli, M. D.; Hamers, R. J.; Murphy, C. J.; Haynes, C. L. Impacts of gold nanoparticle charge and ligand type on surface binding and toxicity to Gram-negative and Gram-positive bacteria. *Chem. Sci.,* **2015,** *6,* 5186-5196.

45. Brezonik, P. L.; Arnold, W. A., *Water chemistry: An introduction o the chemistry of natural and engineered aquatic systems*. Oxford University Press: New York, 2011.

46. Malvern Instruments. *Intensity-volume-number: What size is correct*; Technical Note MRK1357-01.

47. Smoluchowski, M. V., Handbuchder elektrizitat und des magnetismus. In *Electrische endosmose und stro-mungsstrome*, Greatz, L., Ed. Barth: Leipzig, 1921; Vol. 2, pp 62-366.

48. Ohshima, H. Electrokinetics of soft particles. *Colloid. Polym. Sci.,* **2007,** *285,* 1411-1421.

49. Reviakine, I.; Johannsmann, D.; Richter, R. P. Hearing what you cannot see and visualizing what you hear: Interpreting quartz crystal microbalance data from solvated interfaces. *Anal. Chem.,* **2011,** *83,* 8838-8848.

50. Sauerbrey, G. Verwendung von schwingquarzen zur wagung dunner schichten und zur mikrowagung. *Zeitschrift Fur Physik,* **1959,** *155,* 206-222.

51. Cho, N. J.; Kanazawa, K. K.; Glenn, J. S.; Frank, C. W. Employing two different quartz crystal microbalance models to study changes in viscoelastic behavior upon transformation of lipid vesicles to a bilayer on a gold surface. *Anal. Chem.,* **2007,** *79,* 7027-7035.

52. Quevedo, I. R.; Olsson, A. L.; Tufenkji, N. Deposition kinetics of quantum dots and polystyrene latex nanoparticles onto alumina: Role of water chemistry and particle coating. *Environ. Sci. Technol.,* **2013,** *47,* 2212-2220.

53. Chen, K. L.; Elimelech, M. Interaction of fullerene (C_{60}) nanoparticles with humic acid and alginate coated silica surfaces: Measurements, mechanisms, and environmental implications. *Environ. Sci. Technol.,* **2008,** *42,* 7607-7614.

54. Quevedo, I. R.; Tufenkji, N. Influence of solution chemistry on the deposition and detachment kinetics of a CdTe quantum dot examined using a quartz crystal microbalance. *Environ. Sci. Technol.,* **2009,** 3176-3182.

55. Richter, R.; Mukhopadhyay, A.; Brisson, A. Pathways of lipid vesicle deposition on solid surfaces: A combined QCM-D and AFM study. *Biophys. J.,* **2003,** *85,* 3035-3047.

56. Keller, C. A.; Kasemo, B. Surface specific kinetics of lipid vesicle adsorption measured with a quartz crystal microbalance. *Biophys. J.,* **1998,** *75,* 1397-1402.

57. Qiu, T. A.; Nguyen, T. H.; Hudson-Smith, N. V.; Clement, P. L.; Forester, D. C.; Frew, H.; Hang, M. N.; Murphy, C. J.; Hamers, R. J.; Feng, Z. V.; Haynes, C. L. Growth-based bacterial viability assay for interference-free and high-throughput toxicity screening of nanomaterials. *Anal. Chem.,* **2017,** *89,* 2057-2064.

58. Gregory, J. Rates of flocculation of latex particles by cationic polymers. *J. Colloid Interface Sci.,* **1973,** *42,* 448-456.

59. Yu, W. L.; Bouyer, F.; Borkovec, M. Polystyrene sulfate latex particles in the presence of poly(vinylamine): Absolute aggregation rate constants and charging behavior. *J. Colloid Interface Sci.,* **2001,** *241,* 392-399.

60. Elimelech, M.; Nagai, M.; Ko, C.-H.; Ryan, J. N. Relative insignificance of mineral grain zeta potential to colloid transport in geochemically heterogeneous porous media. *Environ. Sci. Technol.,* **2000,** *34,* 2143-2148.
61. Jones, E. H.; Su, C. Transport and retention of zinc oxide nanoparticles in porous media: Effects of natural organic matter versus natural organic ligands at circumneutral pH. *J. Hazard. Mater.,* **2014,** *275,* 79-88.
62. Han, Y.; Kim, D.; Hwang, G.; Lee, B.; Eom, I.; Kim, P. J.; Tong, M.; Kim, H. Aggregation and dissolution of ZnO nanoparticles synthesized by different methods: Influence of ionic strength and humic acid. *Colloids Surf., A,* **2014,** *451,* 7-15.
63. Zimmermann, R.; Kuttner, D.; Renner, L.; Kaufmann, M.; Zitzmann, J.; Muller, M.; Werner, C. Charging and structure of zwitterionic supported bilayer lipid membranes studied by streaming current measurements, fluorescence microscopy, and attenuated total reflection Fourier transform infrared spectroscopy. *Biointerphases,* **2009,** *4,* 1-6.
64. Chen, K. L.; Elimelech, M. Aggregation and deposition kinetics of fullerene (C_{60}) nanoparticles. *Langmuir,* **2006,** *22,* 10994-11001.
65. Zhang, X.; Yang, S. Nonspecific adsorption of charged quantum dots on supported zwitterionic lipid bilayers: Real-time monitoring by quartz crystal microbalance with dissipation. *Langmuir,* **2011,** *27,* 2528-2535.
66. Moghadam, B. Y.; Hou, W. C.; Corredor, C.; Westerhoff, P.; Posner, J. D. Role of nanoparticle surface functionality in the disruption of model cell membranes. *Langmuir,* **2012,** *28,* 16318-16326.
67. Kuech, T. R. Biological interactions and environmental transformations of nanomaterials. Ph. D. Dissertation, University of Wisconsin-Madison, 2015.
68. Troiano, J. M.; Kuech, T. R.; Vartanian, A. M.; Torelli, M. D.; Sen, A.; Jacob, L. M.; Hamers, R. J.; Murphy, C. J.; Pedersen, J. A.; Geiger, F. M. On electronic and charge interference in second harmonic generation responses from gold metal nanoparticles at supported lipid bilayers. *J. Phys. Chem. C,* **2016,** *120,* 20659-20667.
69. Zhang, M.; Soto-Rodríguez, J.; Chen, I. C.; Akbulut, M. Adsorption and removal dynamics of polymeric micellar nanocarriers loaded with a therapeutic agent on silica surfaces. *Soft Matter,* **2013,** *9,* 10155.
70. Frost, R.; Jonsson, G. E.; Chakarov, D.; Svedhem, S.; Kasemo, B. Graphene oxide and lipid membranes: Interactions and nanocomposite structures. *Nano Lett.,* **2012,** *12,* 3356-3362.
71. Kirschner, K. N.; Lins, R. D.; Maass, A.; Soares, T. A. A glycam-based force field for simulations of lipopolysaccharide membranes: Parametrization and validation. *J. Chem. Theory Comput.,* **2012,** *8,* 4719-4731.
72. Clifton, L. A.; Holt, S. A.; Hughes, A. V.; Daulton, E. L.; Arunmanee, W.; Heinrich, F.; Khalid, S.; Jefferies, D.; Charlton, T. R.; Webster, J. R.; Kinane, C. J.; Lakey, J. H. An accurate *in vitro* model of the *E. coli* envelope. *Angew. Chem. Int. Ed.,* **2015,** *54,* 11952-11955.
73. Nikaido, H. Molecular basis of bacterial outer membrane permeability revisited. *Microbiology and Molecular Biology Reviews,* **2003,** *67,* 593-656.
74. Liu, B.; Knirel, Y. A.; Feng, L.; Perepelov, A. V.; Senchenkova, S. N.; Reeves, P. R.; Wang, L. Structural diversity in *Salmonella* O antigens and its genetic basis. *FEMS Microbiol. Rev.,* **2014,** *38,* 56-89.
75. Su, G.; Zhou, H.; Mu, Q.; Zhang, Y.; Li, L.; Jiao, P.; Jiang, G.; Yan, B. Effective surface charge density determines the electrostatic attraction between nanoparticles and cells. *J. Phys. Chem. C,* **2012,** *116,* 4993-4998.

741 76. You, C. C.; Miranda, O. R.; Gider, B.; Ghosh, P. S.; Kim, I. B.; Erdogan, B.; Krovi, S.
742 A.; Bunz, U. H.; Rotello, V. M. Detection and identification of proteins using nanoparticle-
743 fluorescent polymer 'chemical nose' sensors. *Nat. Nanotechnol.,* **2007,** *2,* 318-323.
744 77. Goodman, C. M.; McCusker, C. D.; Yilmaz, T.; Rotello, V. M. Toxicity of gold
745 nanoparticles functionalized with cationic and anionic side chains. *Bioconjugate Chem.,* **2004,**
746 *15,* 897-900.

747

748

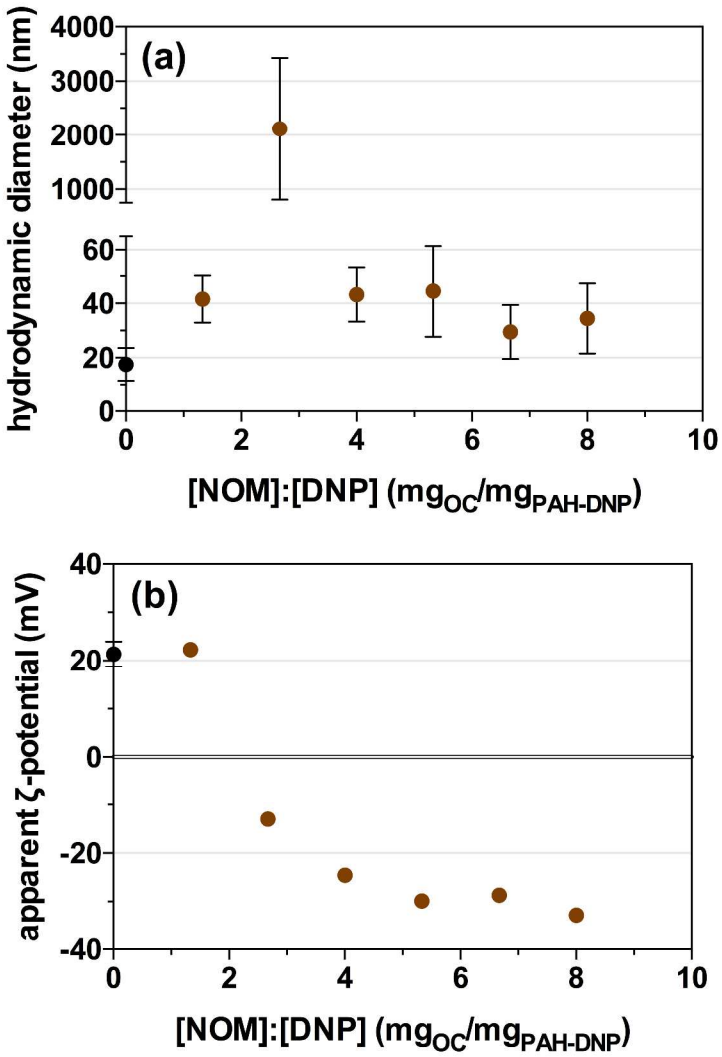

749

750

751 **Figure 1.** PAH-DNP (a) number-averaged hydrodynamic diameters and (b) apparent ζ-potentials
752 as a function of Suwannee River NOM-to-nanoparticle concentration ratio in 0.025 M NaCl
753 buffered to pH 7.4 with 0.002 M HEPES. Error bars represent one standard deviation of five
754 replicate measurements. In some cases error bars in the apparent ζ-potential plot fall within the
755 size of the marker.

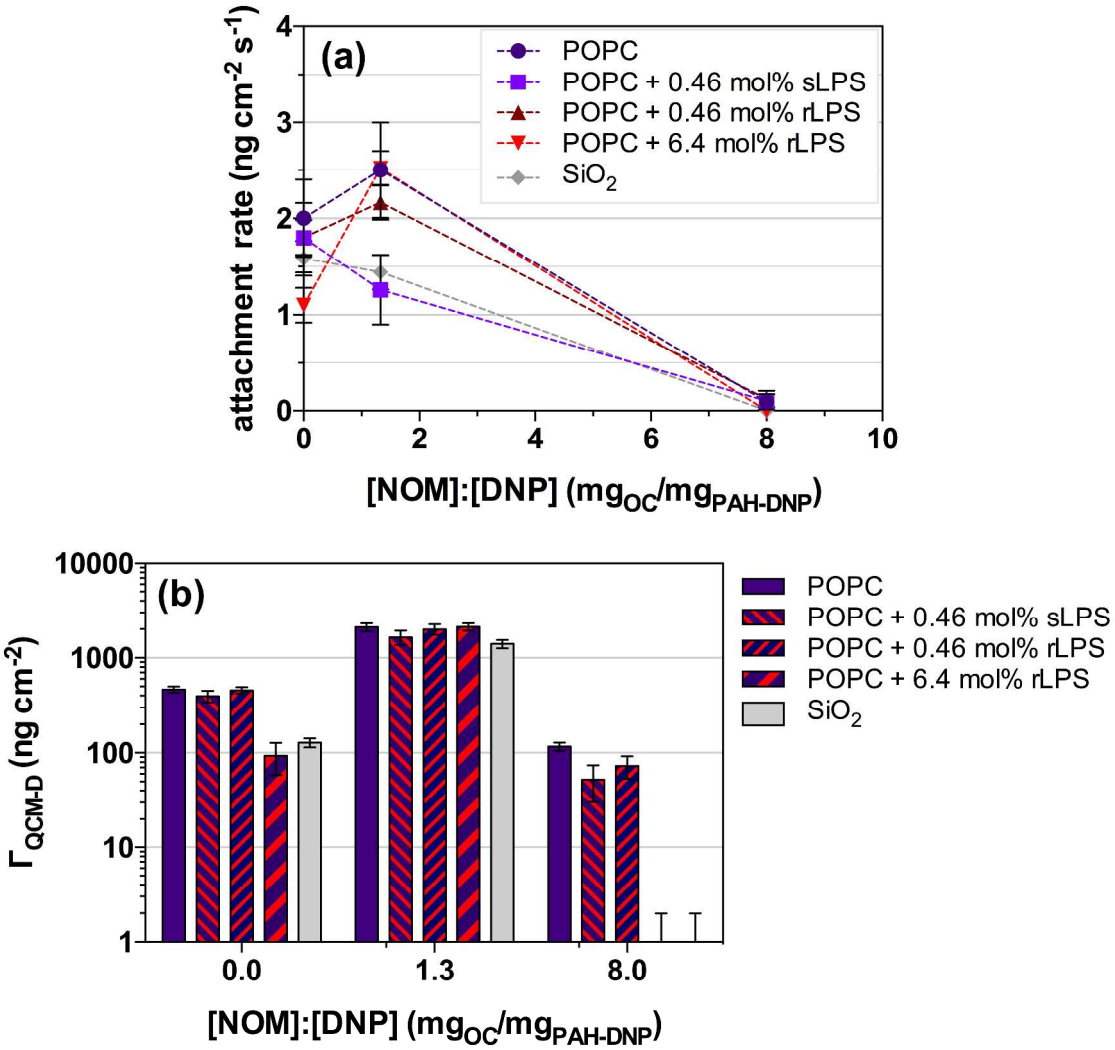

Figure 2. Natural organic matter (NOM) influences the attachment of PAH-DNP to supported lipid bilayers composed of the zwitterionic phospholipid POPC alone or with the indicated amounts of smooth or rough lipopolysaccharide (LPS). (a) Initial rates of PAH-DNP attachment to and (b) acoustic surface mass density (Γ_{QCM-D}) at 20 min for the indicated bilayers and SiO_2 as a function of NOM concentration. Attachment rates defined as the first derivative of the change in acoustic surface mass density with respect to time over the first 30 seconds of attachment. Dotted lines are to guide the eye. Acoustic surface mass densities calculated from the Sauerbrey equation[50] (in all cases $\Delta D_n/(\Delta f_n/n) < 0.4 \times 10^{-6}$ Hz^{-1})[49]. Symbols represent means of at least triplicate measurements; error bars denote one standard deviation. Experiments used 1 nM (number concentration) of PAH-DNPs in 0.025 M NaCl buffered to pH 7.4 with 0.002 M HEPES with the indicated amount of Suwannee River NOM at 25 °C. Numerical data for initial attachment rates and Γ_{QCM-D} are presented in Tables S1 and S8, respectively. Abbreviations: PAH-DNP, diamond nanoparticles functionalized with poly(allylamine HCl); POPC, 1-palmitoyl-2-oleoyl-*sn*-glycero-3-phosphocholine; rLPS, rough lipopolysaccharide; sLPS, smooth lipopolysaccharide.

773

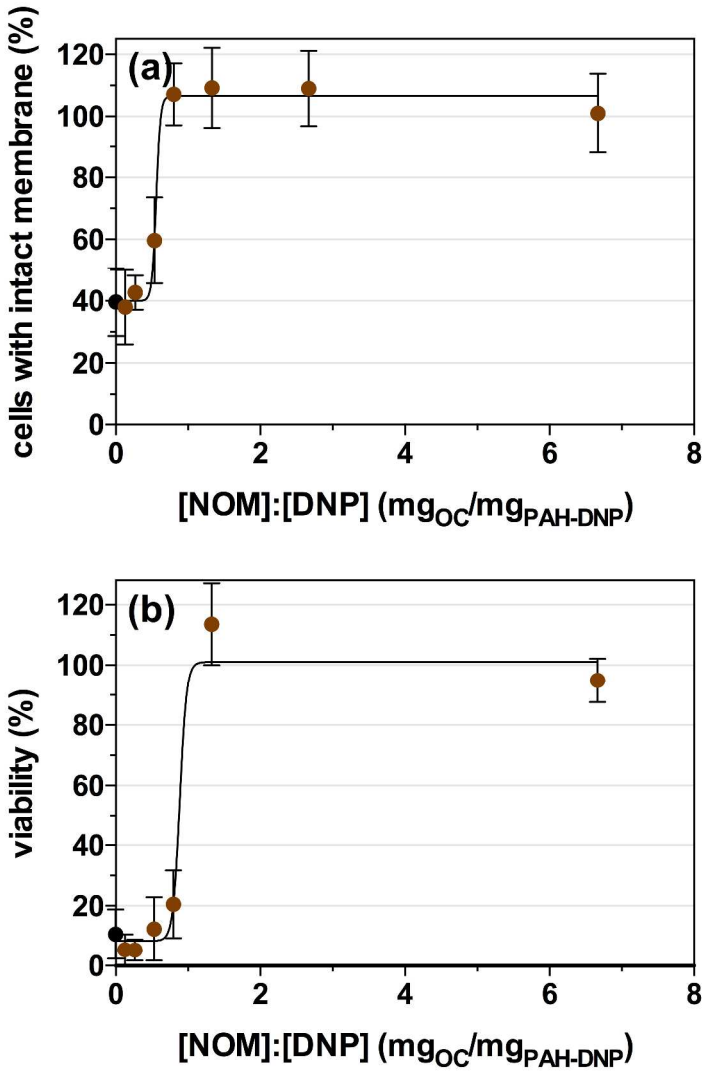

774

775
776

777 **Figure 3.** The influence of NOM-to-DNP ratio on (a) membrane damage and (b) toxicity to
778 *Shewanella oneidensis* by 1 nM PAH-DNP. Experiments were performed in 0.025 M NaCl
779 buffered with 0.002 M HEPES to pH 7.4.

TOC